EFFECT OF PLASMA ELECTROLYTIC OXIDATION TREATMENT ON CORROSION BEHAVIOR OF AZ91D, AM50, AE42 AND MRI 230D MAGNESIUM ALLOYS

Barbara Kazanski[1], Alex Lugovskoy[2], Michael Zinigrad[3]

[1]*Department of Chemical Engineering, Ariel University, Israel, barbarak@ariel.ac.il*
[2]*Department of Chemical Engineering, Ariel University, Israel, lugovsa@ariel.ac.il*
[3]*Department of Chemical Engineering, Ariel University, Israel, rector@ariel.ac.il*

Keywords: Magnesium alloys, Plasma electrolytic oxidation, micro arc oxidation, corrosion protection, oxide layer;

Abstract

Corrosion behavior of an advanced special magnesium alloy MRI 230D (Magnesium Research Institute, Beer-Sheva) as compared to the commercially available zinc-, manganese- and rare earth- containing alloys was studied. The representatives of the appropriate groups were AZ91D, AM50, and AE42 alloys, respectively.

The applicability of Plasma Electrolytic Oxidation treatment for the corrosion protection of all four of magnesium alloys in 3.0 wt% NaCl aqueous solution saturated with $Mg(OH)_2$, and corrosion behavior of these alloys was studied in this work by several electrochemical and non-electrochemical techniques. The corrosion process of all the alloys before and after PEO treatment was evaluated by open circuit potential (OCP) measurements, electrochemical impedance spectroscopy (EIS), linear polarization tests, linear sweep voltammetry (Tafel extrapolation) and chemical methods, namely mass loss and hydrogen evolution. Corrosion rates for each method were calculated and compared, and the morphology of corroded surface studied.

According to the tests results, the protection by the PEO lowers the rate of corrosion and shifts the corrosion potential to a more noble value for all four alloys. An attempt to explain the influence of the PEO process on the corrosion behavior of the alloys was made. However, the localized character of corrosion causes some deviations in the results obtained even by the same method.

Introduction

Magnesium and its alloys are low-density, durable, weldable and recyclable, which makes them very popular in different industries. Withal, their defenselessness against corrosion and poor wear resistance, [1] require the production of surface protective layers. Some of the technologies that protect magnesium alloys, such as chromate conversion coating, are failing to meet the current environmental protection requirements [2]. Therefore lately, the interest in Plasma Electrolytic Oxidation (PEO), is an environmentally friendly technology, is continually growing in both industry and

science [3]. PEO is related to the conventional anodizing process. However, anodizing normally can produce only relatively thin oxides, while PEO is capable of providing much denser and harder surface structure [4]. During anodizing process, the growing oxide layer creates considerable resistance to the electric current until the process stops. Compared to that, in the Plasma Electrolytic Oxidation process, much higher voltages are used, which creates micro-plasma discharges that can break the oxide layer and the layer thickness continues to grow until a much thicker oxide layer forms.

The most acceptable mechanism of the PEO process was proposed in 1999 by A. L. Yerokhin *et al.* [5]. According to this mechanism, PEO process can be divided into two well-distinguished stages. At the beginning of the PEO process, a massive gas evolution from the sample's surface occurs, causing the formation of a vapor plasma envelope wreathing the specimen. This stage is characterized by the fast growth of the oxide layer and therefore rapid growth of the anodic voltage. After the oxide layer reaches critical thickness, the second stage of the oxidation begins. The anodic voltage is high enough to initiate ionization processes in the vapor envelope and to cause electrical breakdowns on the sample surface [5]. The overall oxide layer formation process can be described by the following three stages: (1) "traditional" metal anodizing, (2) formation of a dielectric barrier layer preventing the further anodizing, and (3) dielectric breakdown caused by the plasma discharges, when the temperature in the oxide layer increases to >1000°C [6] and fresh portions of the electrolyte are injected through the breakdown channels to the metal surface.

Over past two decades, a large number of studies were conducted with the purpose of understanding how different experimental setups and substrate compositions affect the characteristics of the obtained oxide layers [7-11]. When magnesium alloys are oxidized, various oxide phases containing primarily MgO and different oxides of an alloy itself are generated around the plasma discharge channels. The mechanical properties of the oxidized layer, such as hardness, porosity, and others, depend mainly on the ratio of these phases. For example, according to E. Cakmak *et al.* [12], magnesium alloys containing zinc (AZ series) demonstrate better electrochemical and mechanical properties of PEO produced oxide layers than alloys containing manganese (AM series). Therefore, for some manganese containing magnesium alloys, for example, MRI series, other alloying elements (such as calcium, tin, and strontium) were added.

The MRI series of magnesium alloys are new and belong to the advanced materials, developed to address the need for elevated creep resistance for sand mold casting and pressure die casting. Alloy MRI 230D was designed for applications in the automotive industry, such as cylinder blocks, operating at temperatures up to 190°C, and for other high-pressure die casting applications. This alloy presents excellent creep resistance combined with good castability and high strength [13].

This study aims to investigate the effect of Plasma Electrolytic Oxidation on the corrosion resistance of different magnesium alloys. Another purpose of this research is to

obtain a sustainable magnesium corrosion mechanism.

Experimental

High-pressure die-cast MRI 230D, AZ91D, AM50, and AE42 magnesium alloys, whose chemical composition can be found in Table 1, were cut into rectangular flat plates, polished with #300, #600, #1000 grit diamond abrasive paper, degreased ultrasonically in MRC D80H bath in tap water with soap for 10 min and dried with acetone.

Table 1.
Chemical composition of MRI 230D, AZ91D, AM50, AE42 magnesium alloys in wt%.

Element	Al	Zn	Mn	other				Mg
MRI 230D	6.3-7.2	0.08 max	0.15-0.4	Sn	Sr	Ca		Bal.
				0.3-1.2	0.05-0.4	1.8-2.6		
AZ91D	8.5-9.5	0.35-1.0	0.15-0.5	Cu	Si			Bal.
				0.03 max	0.1			
AM50	4.4-5.4	0.22	0.26-0.6	Cu	Si			Bal.
				0.01 max	0.1			
AE42	4.0	-	0.1 max	La	Ce	Th	Nd	Bal.
				0.6	1.2	0.6	0.4	

The electrolyte for the PEO contained 0.05 mol/L Na_2SiO_3 (pentahydrate, Spectrum, practical grade, silicate index n = 1), 0.05mol/L KOH (Finkelman Chemicals, technical grade) and 0.05 mol/L KF (Merck, 99%) in tap water. All the procedures were performed at room temperature with only passive cooling by a 50 L water tank, in which the 3L PEO cell was set. The maximal heating in the course of the oxidation was 2-3°C, and no influence of these temperature changes was observed. The oxidation was performed in AC mode by 50 Hz sew edged voltage at the average current density of approximately 10.0 ± 2.0 A / dm^2 on a home-made 40 kVA PEO station, for 30 minutes.

Conductivities and pH of the electrolytes were measured by a YK-2005WA pH/CD meter before, and after oxidation, the thickness of oxide layers was first roughly measured by MiniTest 730 with SIDSP Thickness gauge and then more precisely by SEM. The surface morphology structure and composition, as well as samples cross-sections, were inspected on scanning electron microscope (SEM, JEOL JSM-6510LV) and electron dispersive spectroscopy (EDS, Thermo scientific NS7).

The electrochemical behavior of all the samples was studied on Ivium Potentiostat in the three-electrode cell arrangement, during the exposure to 3% NaCl solution saturated with $Mg(OH)_2$. The non-oxidized rectangular plates of the alloys were polished, and all the samples (oxidized and pristine) were degreased with acetone, dried by air and packed into a parafilm so that only 1.84 cm^2 area was exposed to the corrosion medium. Thus prepared specimens were left in a standard three-electrode cell (Ag|AgCl in sat. KCl solution was used as the reference electrode, and a Pt wire served as the counter

electrode) until a steady state corrosion potential was achieved. After the achievement of a stable corrosion potential, electrochemical measurements such as Electrochemical Impedance Spectroscopy (EIS), Linear Polarization Resistance (LP) and Tafel extrapolation were performed.

Gravimetric measurements were performed using rectangular oxidized and pristine MRI 230D, AM50, AE42, and AZ91D samples, immersed in 3% NaCl solution saturated with $Mg(OH)_2$. The working area and the initial weight of the specimens were measured prior the tests. Once the test was finished, the samples were extracted, rinsed with acetone, etched in CrO_3 + $AgNO_3$ solution to remove the corrosion products, dried in hot air, and then weighed again to calculate the mass loss per unit surface area. In order to obtain further information, during the gravimetric test, evolved hydrogen was collected using turned up-side-down funnel and biretta.

Results and Discussion

The oxidized and pristine samples of all of the alloys (MRI 230D, AZ91D, AM50, AE42) were immerse in 3% NaCl saturated with $Mg(OH)_2$ solution to achieve steady corrosion potentials (OCP). As is seen from Fig. 1 both pristine and oxidized samples have some potential drops over time that are consistent with the formation of a new corrosion pits. Oxidized samples have more potential drops than pristine ones and it takes longer to achieve steady potential values. In addition, equilibrium potential of the oxidized samples is usually lower than initial potential, while for the pristine samples, the opposite observation can be made. The explanation for these phenomena is very simple: for oxidized samples, equilibrium potential is achieved after corrosion pits are form. Corrosion potential of the untacked surface layer will always be higher than for the damaged one. However, it isn't the case for the pristine samples. Pristine samples are polished before being immerse into electrolyte solution. Mechanical polishing of the samples can damage the sample surface and therefore lead to lower initial potential values [14]. After immersion into electrolyte, damage surface reacts, and potentials values rise again with formation of partially passive oxide layer.

For all alloys the OCP values of oxidized samples were nobler than of pristine ones (Table 2). However, while pristine MRI 230D, AM50 and AE42 show almost identical potential values, pristine AZ91D corrosion potential is less negative, which means that AZ91D alloy is more corrosion resistant than other examined alloys. AE42 alloy shows the greatest effect of oxidation process on corrosion potential – although the OCP value of pristine sample is almost identical to MRI 230D and AM50 values, the OCP value of oxidized sample is approaching AZ91D corrosion potential value.

Table 2.
Open circuit potentials (*vs.* KCl saturated Ag|AgCl) of MRI 230D, AZ91D, AM50 and AE42 magnesium alloys in 3% NaCl solution saturated with $Mg(OH)_2$.

Alloy	OCP of oxidized sample	OCP of pristine sample
MRI 230D	-1.474 V	-1.490 V
AZ91D	-1.453 V	-1.468 V
AM50	-1.467 V	-1.493 V
AE42	-1.454 V	-1.491 V

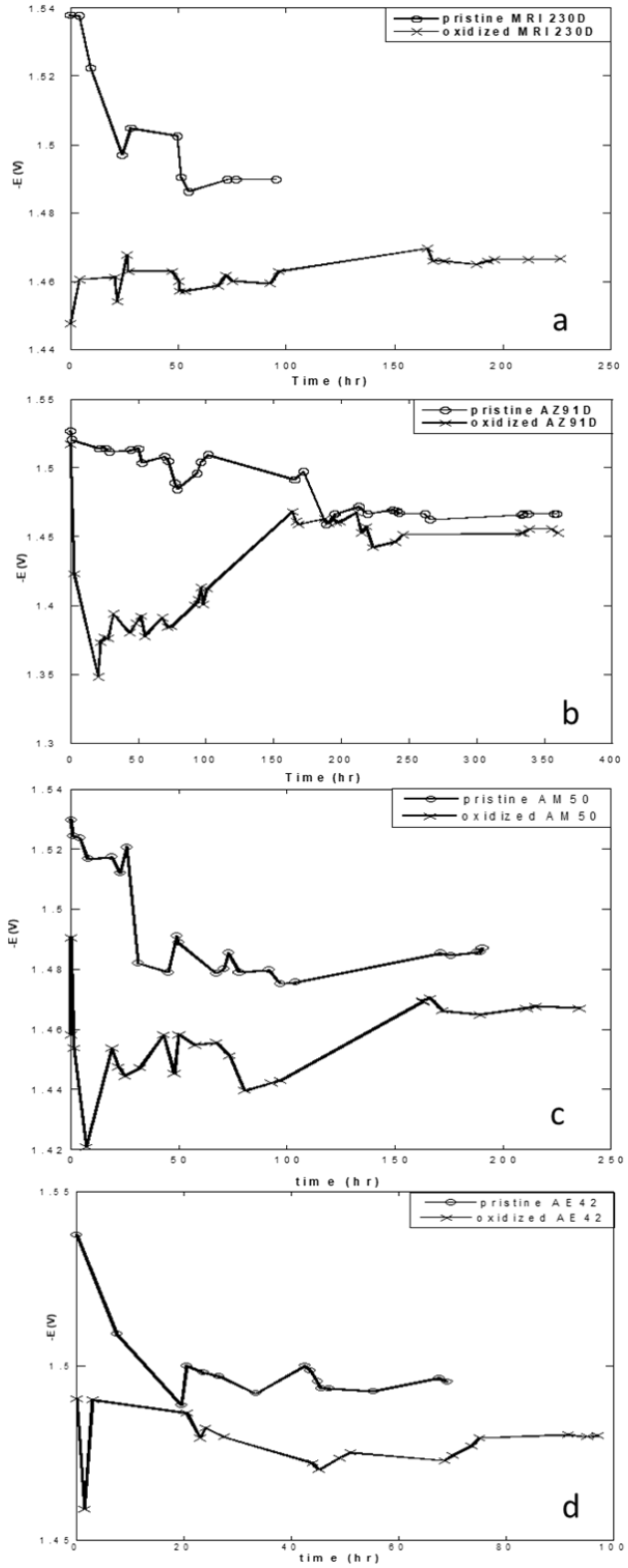

Fig. 1. Stabilization of the corrosion potential (vs. Ag|AgCl) of (a) MRI 230D, (b) AZ91D, (c) AM50 and (d) AE42 alloys in 3% NaCl saturated with $Mg(OH)_2$.

Fig. 2 shows the Nyquist impedance plots of untreated and oxidized alloys after the achievement of steady state potentials. All untreated alloys demonstrated a single capacitive arc at high and intermediate frequencies, which can be attributed to the charge transfer reaction of the magnesium corrosion process, and an inductive loop at low frequencies, which can be explained as sorption of some ions on the metal surface. For the oxidized alloys, the behavior is more complex, because in addition to the inductive loop, the capacitive loop is divided into two.

Two capacitive loops imply that the electrochemical processes occur both at metal-oxide inter phase and inside the oxide layer. However, while those two loops are very distinguished for MRI 230D and AM50 alloys, they are negligible for AZ91D and AE42 alloys.

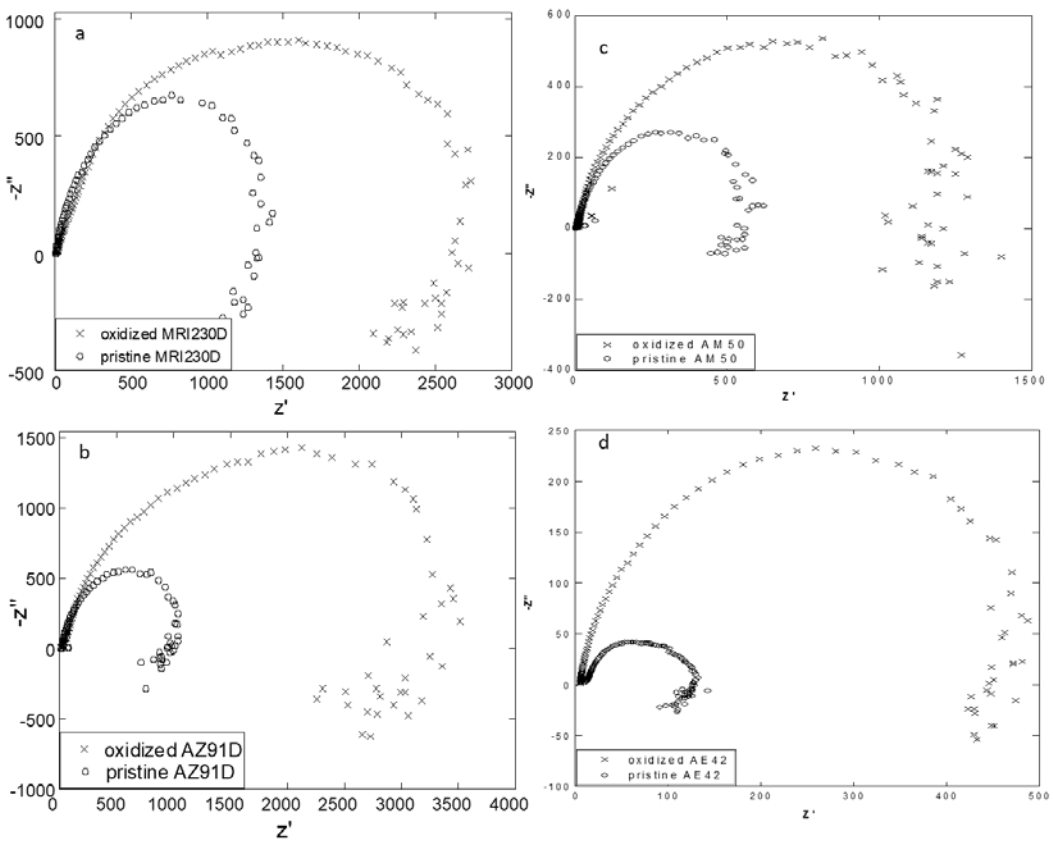

Fig. 2. Typical EIS Nyquist plots for (a) MRI 230D, (b) AZ91D, (c) AM50 and (d) AE42 alloys in 3% NaCl saturated with $Mg(OH)_2$.

The diameter of the capacitive arc is closely related to the corrosion rate and therefore it is clear that PEO process improve corrosion performance of studied alloys.

We assume the following model for the observed phenomena (Fig. 3): one charge transfer process occurs at the surface of the alloy and is can be modeled in the regular manner as $R_{ct}C_{dl}$, where R_{ct} is the charge transfer resistance and C_{dl} is the double layer capacitance. On the surface of the pristine alloys loose oxide layers formed by the corrosion product present an additional resistance R_{tr} in series with an inductance L due to sorption of ions from the electrolyte. The circuit CPE-Rox describes the second time-

constant process. Hypothetically, we might assume this second process to the further oxidation of the intermediate univalent Mg^+, whose participation in the corrosion of magnesium is postulated by many authors. [15] Oxidized alloys are coated with much thicker and denser porous oxide layer, therefore the contribution of the processes in it must be more significant. The proposed equivalent circuit R(QR(LR))(CR) is similar to R(CR)(QR(LR)) proposed by others for the corrosion of magnesium alloy [16], but is better based on the structure of real systems. The corresponding fit parameters are given in Table 3.

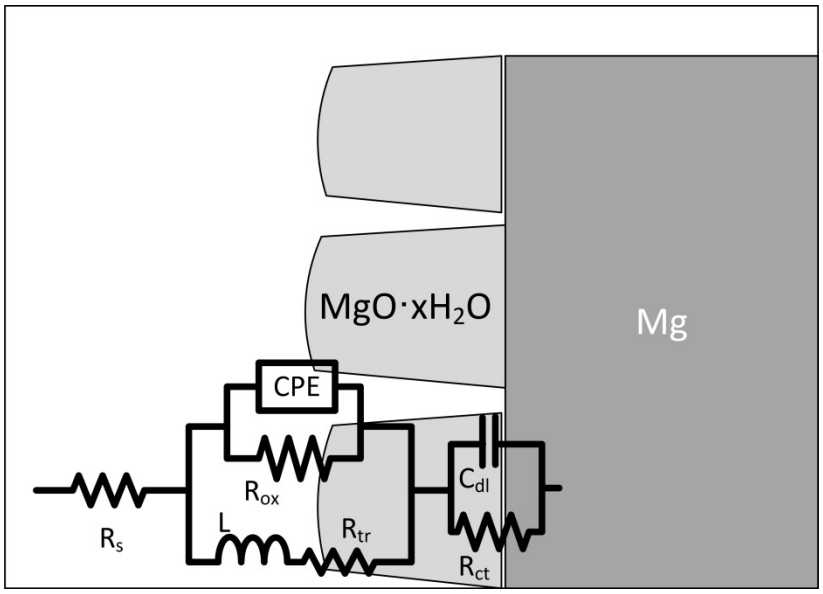

Fig. 3. An equivalent circuit best fit to the measured EIS spectra.

Table 3.
Fit parameters of the measured EIS to the equivalent scheme shown in Fig. 3

alloy		R_S, Ω	R_{ct}, Ω	C_{DL}, F	R_{ox}, Ω	L, H	R_{tr}, Ω	C_{CPE}, F	n_{CPE}
MRI 230D	pristine	9.09	1107	$7.63\cdot10^{-5}$	474.8	205.4	0.01	$1.26\cdot10^{-4}$	0.840
	oxidized	14.07	750.2	$1.24\cdot10^{-4}$	2141	2681	3471	$1.97\cdot10^{-5}$	0.774
AZ91D	pristine	21.1	2.27	$7.18\cdot10^{-5}$	1768	927.6	2948	$9.70\cdot10^{-5}$	0.908
	oxidized	9.46	1.922	$1.81\cdot10^{-5}$	4925	814.6	715.8	$1.95\cdot10^{-4}$	0.556
AM50	pristine	10.8	565.1	$5.44\cdot10^{-6}$	274.6	111.3	112.3	$2.23\cdot10^{-4}$	0.808
	oxidized	23.1	289.4	$6.01\cdot10^{-5}$	972.4	244.0	184.5	$3.52\cdot10^{-4}$	0.441
AE42	pristine	31.6	91.9	$9.32\cdot10^{-5}$	1428	626.3	1974	$8.88\cdot10^{-5}$	0.939
	oxidized	12.1	1767	$1.05\cdot10^{-4}$	1699	431.3	888.5	$2.83\cdot10^{-4}$	0.674

As is seen from Table 3, there are some noticeable differences between the pristine and oxidized alloys: for all four alloys, R_{ox} values are significantly higher for the oxidized samples than for pristine ones, which may hint that the charge transfer occurring inside the oxide layer is slower. However, the calculated R_{ct} values supposed to indicate alloy immunity to corrosion process, which is clearly not the case. This means that such an

over-simplified mechanism is not relevant for our system and other processes in the oxide layers have to be considered.

Tafel slopes, corrosion potential and corrosion current were determined from the polarization curves measured in the potential range of ± 0.25V *vs*. a stable corrosion potential. Typical examples of Tafel plots are presented in Fig. 4. The comparison shows that the corrosion potential for oxidized samples is higher than for of the pristine ones, especially for AZ91D alloy. The change in corrosion potential of the oxidized MRI 230D and AM50 alloys is less significant, yet present. Additionally, the corrosion current of the oxidized samples (for all alloys) is lower than for pristine ones. That means that oxidized samples are nobler and less affected by the corrosion, and when corrosion starts it progresses at the slower rate.

The anodic branches of the Tafel plot, for MRI 230D, AZ91D and AE42, are monotonous and show no passivation phenomena in the above potential range. However, the anodic branch of pristine AM50 alloy shows passivation and a break is observed for the cathodic branch of the MRI 230D pristine sample. We assume that this may evidence another reduction process occurring in the system rather than transport phenomena. The values of Tafel slopes and the corresponding corrosion currents for all alloys are presented in Table 4.

Table 4.
Tafel slops parameters of MRI 230D**,** AZ91D, AM50 and AE42 magnesium alloys in 3% NaCl solution saturated with $Mg(OH)_2$.

alloy		E_{corr}, V	j_{corr}, A/cm^2	β_a, V/dec	β_c, V/dec
MRI 230D	pristine	-1.4098	$1.266 \cdot 10^{-5}$	0.130	0.164
	oxidized	-1.3875	$1.572 \cdot 10^{-5}$	0.230	0.339
AZ91D	pristine	-1.3654	$1.121 \cdot 10^{-5}$	0.096	0.275
	oxidized	-1.3480	$1.082 \cdot 10^{-6}$	0.121	0.219
AM50	pristine	-1.4859	$7.322 \cdot 10^{-6}$	0.087	0.177
	oxidized	-1.4567	$7.118 \cdot 10^{-6}$	0.214	0.238
AE42	pristine	-1.4067	$4.737 \cdot 10^{-7}$	0.195	0.083
	oxidized	-1.3632	$2.116 \cdot 10^{-5}$	0.133	0.276

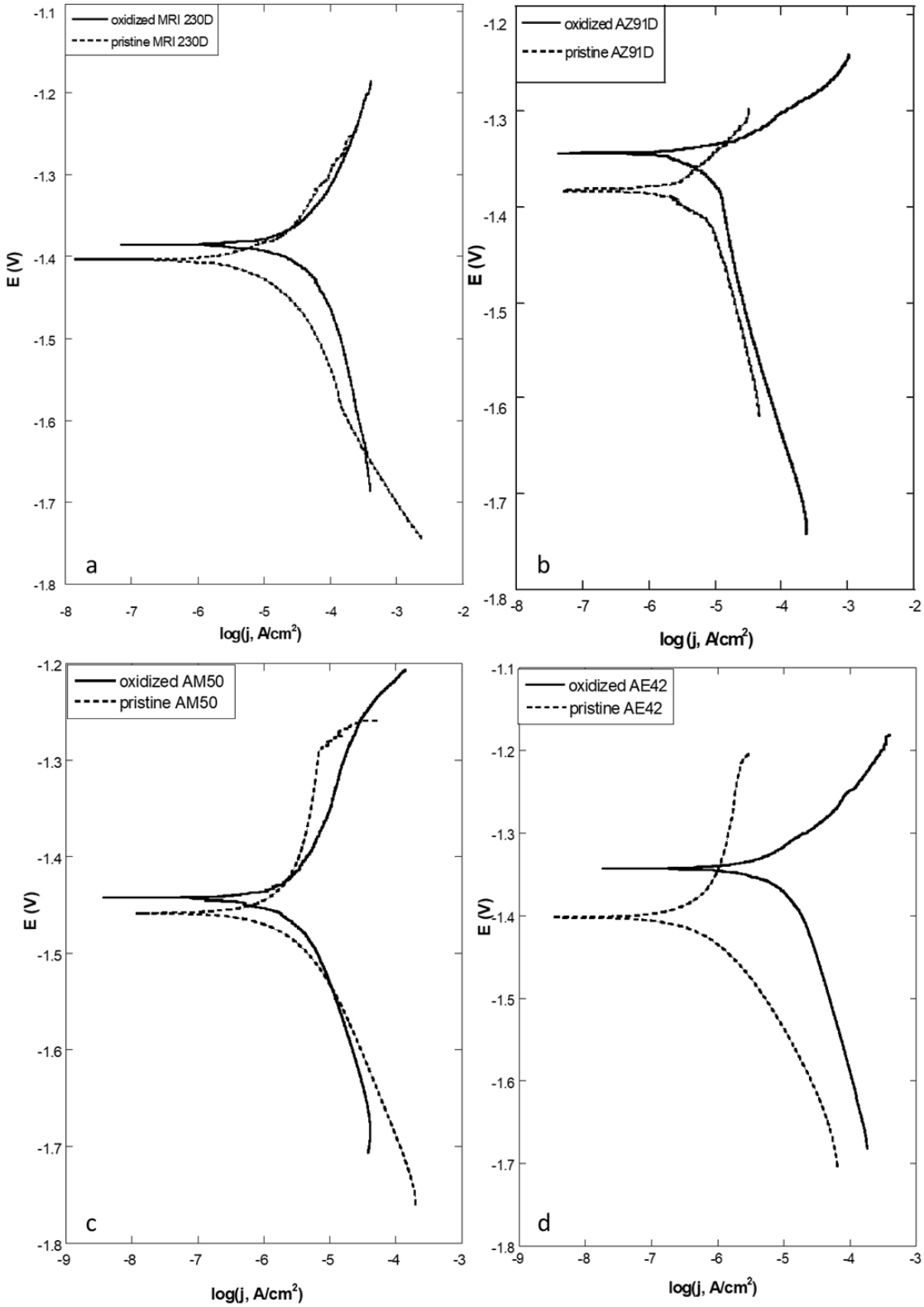

Fig. 4. Typical Tafel polarization plots for (a) MRI 230D, (b) AZ91D, (c) AM50 and (d) AE42 alloys in 3% NaCl saturated with $Mg(OH)_2$.

The values of E_{corr} and j_{corr} (Table 5) were also obtained from linear polarization curves measured in the potential range of E_{ss} ±10mV, both before and after PEO. As is seen from Fig. 5, the deviations of the polarization curve from the linear regression line are negligible in this range.

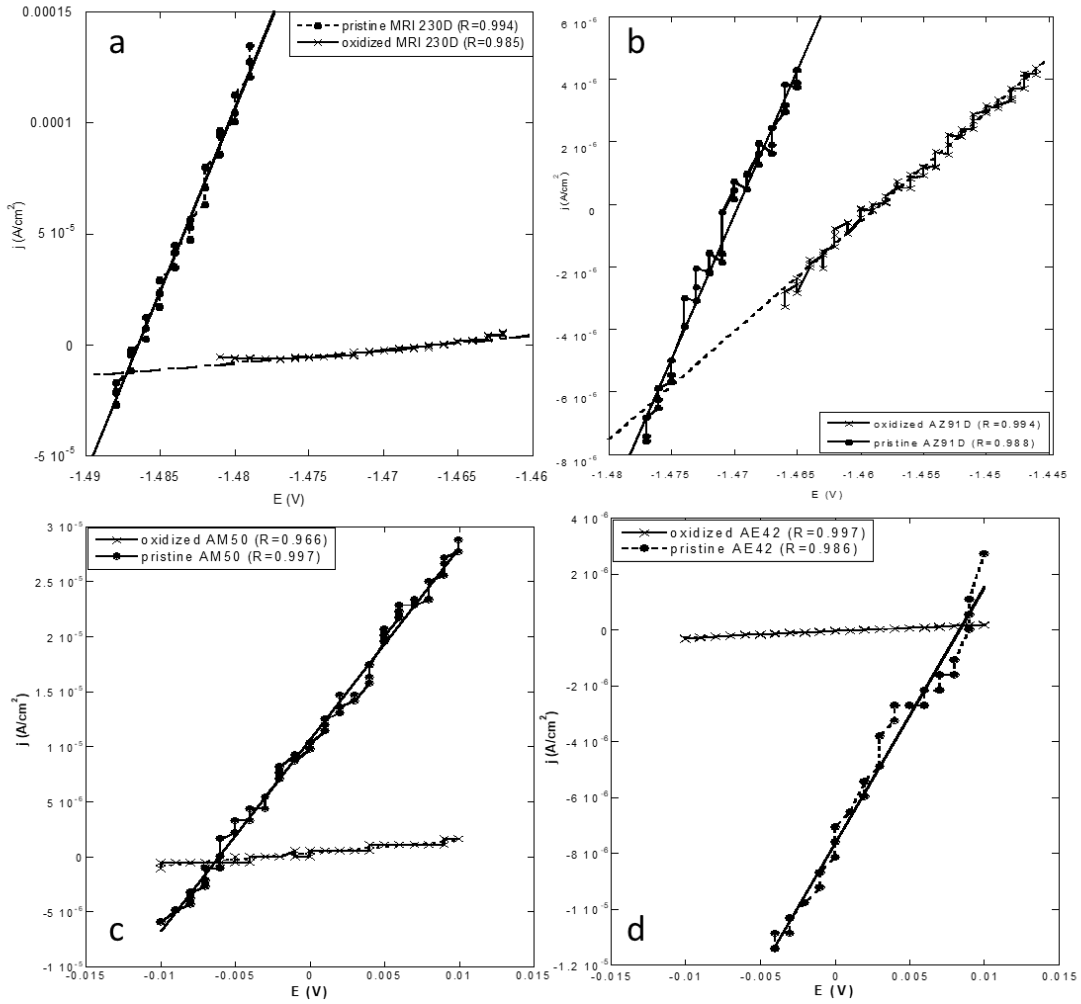

Fig. 5. Typical linear polarization plots for (a) MRI 230D, (b) AZ91D, (c) AM50 and (d) AE42 alloys in 3% NaCl saturated with $Mg(OH)_2$

The values of the cathodic (β_c) and anodic (β_a) Tafel slops from Table 4 were used for the calculation of the Stern-Geary constant B (Eq. 1)

$$B = \frac{\beta_c \cdot \beta_a}{2.3(\beta_c + \beta_a)} \quad (1)$$

And the calculation of polarization resistance R_p (Eq. 2).

$$R_p = \frac{B}{j_{corr}} \quad (2)$$

The calculated Stern-Geary constant values (Table 5) are in good agreement with the literature [17].

Table 5.
Linear polarization parameters of MRI 230D**,** AZ91D, AM50 and AE42 magnesium alloys in 3% NaCl solution saturated with $Mg(OH)_2$.

alloy		B, mV/dec	j_{corr}, A/cm^2	R_p, Ω/cm^2
MRI 230D	pristine	31.53	$3.846\cdot10^{-5}$	819.8
	oxidized	59.58	$2.025\cdot10^{-6}$	29422
AZ91D	pristine	30.94	$1.498\cdot10^{-5}$	2065.4
	oxidized	33.89	$9.362\cdot10^{-6}$	36188
AM50	pristine	33.45	$3.662\cdot10^{-5}$	913.4
	oxidized	48.99	$2.456\cdot10^{-6}$	19947
AE42	pristine	25.31	$4.047\cdot10^{-5}$	625.4
	oxidized	39.02	$2.001\cdot10^{-6}$	19500

Fig. 6 shows the hydrogen evolution *versus* time of oxidized and pristine samples of all four alloys immersed in 3% NaCl saturated with $Mg(OH)_2$ solution.

All samples exhibited almost linear kinetics of hydrogen evolution associated with magnesium dissolution. Untreated MRI 230D sample presented the highest gas evolution rate during the shortest immersion time. In contrast, for oxidized AE42 samples no gas evolution at all was observed for several days. The same observation can be also made for AZ91D alloy. The obtained parameters of the hydrogen evolution and the mass loss of the oxidized and pristine samples over the immersion time are presented in Table 6.

Table 6.
Hydrogen evolution and mass loss parameters of MRI 230D**,** AZ91D, AM50 and AE42 magnesium alloys in 3% NaCl solution saturated with $Mg(OH)_2$.

alloy		t, days	$V(H_2)$, mL	Δm, gr
MRI 230D	pristine	12.42	16.8	0.0196
	oxidized	62.77	1.2	0.0493
AZ91D	pristine	45.76	11.8	0.0140
	oxidized	146.88	12.2	0.0763
AM50	pristine	14.06	17.9	0.0200
	oxidized	132.67	6.9	0.0581
AE42	pristine	26.2	19.3	0.0180
	oxidized	181.3	10.1	0.0047

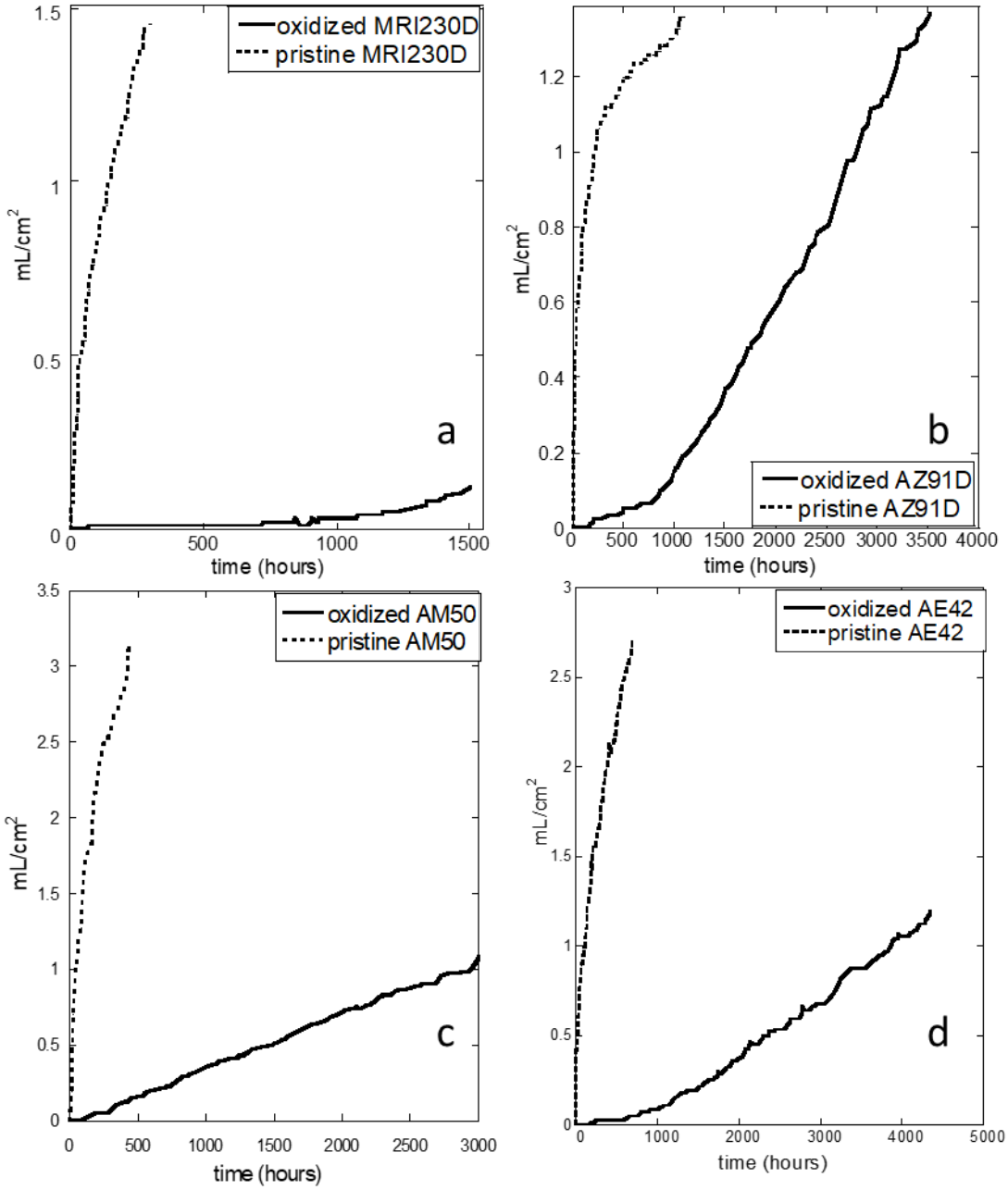

Fig. 6. Plots of the gas evolution rate for (a) MRI 230D, (b) AZ91D, (c) AM50 and (d) AE42 alloys in 3% NaCl saturated with $Mg(OH)_2$

The weight loss corrosion rate, P_W (mm/year), was measured by Eq. 3, according to the literature [18, 19]:

$$P_W = \frac{W_i - W_f}{A \cdot \rho \cdot time} \quad (3)$$

where w_i and w_f (gr) are a sample's initial and final weight, accordingly, A (cm^2) is the surface area of the sample, ρ (gr/cm^3) is the sample's density and *time* is the overall immersion time (years).

The evolved hydrogen was collected during the mass loss test and the average corrosion rate, P_H (mm/year), was calculated by Eq. 4, using the ideal gas law:

$$P_H = \frac{V}{A \cdot time} \quad (4)$$

where V is the total volume of the evolved hydrogen, A (cm^2) is the surface area of the sample and *time* is the overall immersion time (years).

The rates of corrosion measured by different methods are summarized in Table 7.

Table 7. Corrosion rates in mm/year for oxidized and pristine MRI 230D and AZ91D alloys measured by different methods.

alloy		R_{EIS}	R_{Tafel}	R_{LPR}	R_{gas}	$R_{mass\ loss}$
MRI 230D	pristine	5.40	0.27	0.76	0.27	0.23
	oxidized	3.57	0.08	0.08	0.05	0.06
AZ91D	pristine	0.43	0.13	0.29	0.08	0.09
	oxidized	0.39	0.11	0.18	0.02	0.01
AM50	pristine	2.05	0.38	0.16	0.27	0.31
	oxidized	1.68	0.04	0.02	0.02	0.03
AE42	pristine	0.48	0.25	0.35	0.21	0.21
	oxidized	0.37	0.02	0.02	0.01	0.01

As is seen from Table 7, the corrosion of a PEO treated samples is always slower than that of a pristine specimen, for all tested alloys. As expected, mass loss and hydrogen evolution corrosion rates are in a good agreement with each other for all the tested samples. However, in a contrary to the literature, Tafel extrapolation corrosion rates matching better the gravimetric results than linear polarization technique for all the alloys, except AM50. In addition, EIS provided results differentiate from all the other methods. For our specific case, we can assume some explanations to these differences:

1. Both the EIS spectra and the equivalent circuit used here (Figs 2, 3) demonstrate quite clearly that the corrosion process has a very complex mechanism including sorption, diffusion and two charge-transfer steps. The calculation of the corrosion rates is based on the assumption that they are controlled by the charge-transfer resistance R_{ct}. Obviously, the reality is less simple and a mixed control takes place. In addition, another plausible explanation can be, that fit of the EIS equivalent circuit (Fig. 3) is lower than expected.

2. The cathodic Tafel slopes hint that the diffusion of the Red species (presumably, water molecules or OH^--ions) through the film of the corrosion products is retarded and may contribute to the process control type. Presumably, the corrosion process may have a mixed control of the Charge Transfer and the Diffusion steps. If this is the case, all the three electrochemical techniques are more sensible to the rates of the CT process, which is not (the only) rate determining step.

3. The corrosion rates measured by the non-electrochemical techniques (gas evolution and mass loss) are more relevant to the *total* corrosion process. While these techniques cannot give us anything concerning the mechanism, they are much more accurate in the practical sense.

Conclusions

The corrosion of MRI 230D, AZ91D, AM50 and AE42 magnesium alloys was measured by electrochemical and non-electrochemical techniques. The corrosion rates measured by different methods show some discrepancies, especially by EIS technique. For some alloys, the electrochemical techniques provide larger corrosion rates than those measured by the mass loss and gas evolution.

The electrochemical techniques show that the corrosion process is complex and its rate is partially limited by the diffusion of the reducer to the metal surface. The higher values of the corrosion rate calculated from the electrochemical measurements may reflect the faster charge-transfer step rather than the r.d.s.

References

[1] B. A. Shaw, "Corrosion Resistance of Magnesium Alloys", *ASM Handbook*, 13A, 692-695, (2003)

[2] M. Bielewski, "Replacing Cadmium and Chromium", *Research and Technology Organization and NATO*, RTO-AG-AVT-140 (2011), Chp. 23, pp 1-22.

[3] A. Lugovskoy, M. Zinigrad, "Plasma Electrolytic Oxidation of Valve Metals", *Materials Science - Advanced Topics*,(2013), Chp. 4, pp. 85–102. doi:10.5772/54827.

[4] K. Murakami, M. Hino, K.Nakai, S. Kobayashi, A.Saijo, T.Kanadani, "Mechanism of Corrosion Protection of Anodized Magnesium Alloys", Mater.Transact.,49 (5),1057–1064, (2008)

[5] A. L. Yerokhin, X. Nie, A. Leyland, A. Matthews, S. J. Dowey, "Plasma electrolysis for surface engineering", Surf. Coat.Tech. 122, 73-93, (1999).

[6] I. Suminov, P. Belkin, A. Epelfeld, V. Ludin, B. Krit, A. Borisov, "World of materials and technology. Plasma electrolytic surface modification of metals and alloys", *Technosfera*, Moscow, (2011), Vol. 2, p. 25 (in Russian).

[7] B. Kazanski, A. Kossenko, M. Zinigrad, A. Lugovskoy, "Fluoride ions as modifiers of the oxide layer produced by plasma electrolytic oxidation on AZ91D magnesium alloy", App. Surf. Sci.,287,461– 466, (2013)

[8] J. Li, Y. Tian, Z. Cui, Z. Huang, "Effects of rare earths on the microarc oxidation of a magnesium alloy", Rare Metals, 27 (I), 50– 54, (2008)

[9] H. Duan, C. Yan, F. Wang, "Effect of electrolyte additives on performance of plasma electrolytic oxidation films formed on magnesium alloy AZ91D", Electrochim. Acta, 52, 3785–3793, (2007)

[10] R.F. Zhang, D.Y. Shan, R.S. Chen, E.H. Han, "Effects of electric parameters on properties of anodic coatings formed on magnesium alloys", Mater. Chem. and Phys., 107, 356–363, (2008)

[11] C. Blawert, V. Heitmann, W. Dietzel, H.M. Nykyforchyn, M.D. Klapkiv, “Influence of process parameters on the corrosion properties of electrolytic conversion plasma coated magnesium alloys”, Surf. Coat. Tech., 200, 68– 72, (2005)
[12] E. Cakmak, K. C. Tekin, U. Malayoglu, S. Shrestha, “The effect of substrate composition on the electrochemical and mechanical properties of PEO coatings on Mg alloys”, Surf. Coat. Tech., 204, 1305–1313, (2010)
[13] MRI alloys, (n.d.). http://www.dsmag.co.il/?cmd=products.5#MRI Alloys.

[14] G. S. Frankel, “Pitting Corrosion of Metals. A Review of the Critical Factors”, J. Electrochem. Soc., 145 (6), 2186-2198, (1998)

[15] G. Song, A. Atrens, Understanding Magnesium Corrosion - A Framework for Improved Alloy Performance, Adv. Eng. Mater., 5(12), 837-858, (2003)
[16] J. Chen, J. Wang, E. Han, J. Dong and W. Ke, AC impedance spectroscopy study of the corrosion behavior of an AZ91 magnesium alloy in 0.1M sodium sulfate solution, Electrochim. Acta, 52, 3299–3309, (2007)
[17] A.Pardo, S.Feliu Jr., M.C.Merino, R.Arrabal, and M.Matykina, “Electrochemical Estimation of the Corrosion Rate of Magnesium/Aluminium Alloys”, Intern. Journal of Corrosion, vol. 2010, Article ID 953850, eight pages, 2010. doi:10.1155/2010/953850.
[18] Z. Shi, M. Liu, A. Atrens, “Measurement of the corrosion rate of magnesium alloys using Tafel extrapolation”, Corros. Sci., 52, 579–588, (2010)
[19] F. Cao, Z. Shi, J. Hofstetter, P. J. Uggowitzer, G. Song, M. Liu, A. Atrens, “Corrosion of ultra-high-purity Mg in 3.5% NaCl solution saturated with $Mg(OH)_2$”, Corros. Sci., 75, 78–99, (2013)